Talanta 269 (2024) 125481

Contents lists available at ScienceDirect

Talanta

journal homepage: www.elsevier.com/locate/talanta

Terahertz reconfigurable metasensor for specific recognition multiple and mixed chemical substances based on AIT fingerprint enhancement

Lihao Huang [a], Hongyan Cao [a], Lin Chen [a,b,*], Yi Ma [a], Yihan Yang [a], Xiaoyang Liu [a], Wenqi Wang [a], Yiming Zhu [a*], Songlin Zhuang [a]

[a] Terahertz Technology Innovation Research Institute, Shanghai Key Lab of Modern Optical System, University of Shanghai for Science and Technology, Shanghai, 200093, China

[b] The Shanghai Institute of Intelligent Science and Technology, Tongji University, Shanghai, 200092, China

ARTICLE INFO

Handling editor: J. Wang

Keywords:
Terahertz
Plasmonic metasensor
Absorption-induced transparency
Fingerprint detection
Mixed chemical substances

ABSTRACT

Terahertz (THz) fingerprint metasensing is an effective method to identify chemical substances in a rapid and non-destructive way. Currently, two main principles are used in THz metasensing: the change of the real part of permittivity causing the dip resonance frequency deviation, and the fingerprint peak of the imaginary part of permittivity causing the dip resonance splitting (absorption induced transparency, AIT). Most previous work investigated AIT detection for only single chemical substance. The suitable AIT metasensor structure are still required for simultaneously measurement of multiple and mixture chemical substances. In this manuscript, we proposed the N-order concentric rings metasensor for specific recognition multiple and mixed chemical substances based on AIT fingerprint enhancement. The structure has broadband multiple plasmonic resonance dips which are generated by near field dipole resonances. The equivalent circuit model was built to realize the reconfigurable function. Then, 5-order concentric rings structure was designed and fabricated for simultaneously specific recognition of four chemical substances (α-lactose, benzoic acid, vitamin B2 and 2, 5-dichloroanline). The influence of the real and imaginary part of the chemical substances' permittivity on AIT effect had discussed in details. Simulation results indicated that the frequency-deviation of the resonance dip can be stabilized and will not be changed when the concentration of chemical substances is over 20 mg/mL. As shifted plasmonic resonance peaks match the chemical substances' imaginary part of permittivity fingerprint spectra, the perfect AIT effect can be realized. The metasensor can simultaneously and non-destructively conduct a specific detection of α-lactose, benzoic acid, vitamin B2 and 2,5-dichloroanline, and their mixture. The limit of detections of α-lactose, benzoic acid, vitamin B2 and 2,5-dichloroanline are 8.61 mg/mL, 6.96 mg/mL, 7.54 mg/mL and 8.35 mg/mL, respectively. Also, the sensitivity of the metasensor can reach 0.00211, 0.00208, 0.00211 and 0.00219 (unit: 1/mg/mL), respectively. By utilizing one-way analysis of variance method, the possibility of recognition error for each chemical substance is lower than 0.001. Our metasensor provides a novel and accurate platform for THz fingerprint sensing.

1. Introduction

The agricultural products and food are essential to human health and vitality. With the development of modern technologies, there are destructive and non-destructive methods to detect food and agricultural products [1]. For instance, mass spectrometry and liquid chromatography have excellent sensitivity and moderate reproducibility, but they also have problems such as complicated preliminary processing, large sample loss, and relatively high cost and are time consuming [2–5]. Near infrared spectroscopy are common non-destructive technology. However, it is limited by poor reproducibility [6–8]. Terahertz (THz) waves lies between microwaves and far infrared, covering the frequency from 0.1 THz to 10 THz. THz radiation has several advantages. For instance, it has strong transparency in most dielectrics. The photon energy is low and can't cause any damage to biomolecules. In addition, many complex molecules have their vibrational and rotational modes at THz regime

* Corresponding author. Terahertz Technology Innovation Research Institute, Shanghai Key Lab of Modern Optical System, University of Shanghai for Science and Technology, Shanghai, 200093, China.
E-mail address: linchen@usst.edu.cn, ymzhu@usst.edu.cn.

https://doi.org/10.1016/j.talanta.2023.125481
Received 22 August 2023; Received in revised form 19 November 2023; Accepted 23 November 2023
Available online 25 November 2023

which is convenient for biomolecule detection [9]. Generally, the amplitude and the phase of the broadband THz wave with the information of the chemical substances can be acquired by using commercial THz time domain spectroscopy (THz-TDS) system. The refractive index and absorption coefficient of the chemical substances can be further obtained and analysis. For instance, H. Liu et al. obtained the absorption spectra of the explosive RXD by utilized THz-TDS system [10]. Y. Ueno et al. demonstrated a quantitative analysis of amino acids in dietary supplements in THz band [11]. However, this method is not suitable for trace detection due to size mismatch between thin film sample and THz wavelength. Thus, metamaterial has been proposed and analyzed to enhance near field light matter interaction [12,13]. The local field of metamaterial sensor (metasensor) benefits sensitive detection of tiny environment change around the electromagnetic confinement area, resulting in the enhanced sensitivity [14,15].

Up to date, the mechanism of THz metasensors lie in two ways: refractive index sensing and fingerprint peak detection. For refractive index sensing, the change of the chemical substances' permittivity will cause the frequency dip deviation in the transmission spectra. For instance, C. Zhang et al. designed a concentric ring metasensor to detect cell apoptosis of oral cancer cell under the chemotherapy drug treatment [16]. An obvious dip-deviation can be observed in the transmission spectra, and the relative resonant frequency change of the metasensor was linear with refractive index change due to apoptosis. X. Wu et al. designed the metasensors to detect refractive index change of streptavidin–agarose due to solution concentration difference [17]. However, these analysis methods ignore the specific identification of THz fingerprint spectrum of chemical substances. For fingerprint peak detection, by matching the broadband metasensor resonance dip with the chemical substances' narrowband absorption peak, absorption induced transparency (AIT) effect can be excited, which can achieve specific recognition of chemical substances in THz band. For instance, Xie et al. designed a split-ring resonator (SRR) metasensor structure. The structure's characteristic transmission dip matches the absorption peak of L-tartaric, causing the AIT effect which can realize specific detection of L-tartaric [18]. B. Han et al. designed similar metasensor for the fingerprint detection of lactose [19]. However, there still exists some drawbacks: (1) The designed sensor can detect only one selected chemical substance and can't detect multiple chemical substances and their mixture; (2) The real part of chemical substances' permittivity generates the obvious resonance frequency deviation of the metasensor, leading to mismatch between metasensor mode frequency and fingerprint absorption frequency, and resulting in non-excitation of AIT effect. Although Z. Han et al. designed a InSb coupled rod structure to realize a tunable AIT sensor [20], the tunable frequency range is narrow.

In this paper, we proposed the metasensor consisted of N-order concentric rings plasmonic structure to achieve specific multiple fingerprint metasensor. We defined the Mth resonance of N-order concentric rings plasmonic structure in the transmission spectrum (from low frequency to high frequency) as (N, M) mode. Different diameters of the concentric rings have the different dipole resonant modes (frequencies), except that (4, 4) (5, 4) and (5, 5) modes show hybrid modes which are the interaction between dipole mode (caused by single concentric ring) and hexapole mode (caused by outer rings). Due to the near field weak interaction between concentric rings, there exist slight differences between the resonance frequency of a single ring in multiple concentric rings scenario and that in separate scenario. We established the circuit models for N-order concentric rings to explain such near field effect. In our proof-of-principle experiment, we selected N as 5 and carefully optimized parameters to excite four dipole modes which can perfect match the fingerprint absorption spectra of four chemical substances (α-Lactose, Benzoic Acid, Vitamin B2 and 2,5-Dichloroaniline) by considering frequency-shift compensation caused by the real part of the chemical substances' permittivity. The metasensor can specifically and simultaneously detect 4 chemicals (α-Lactose, Benzoic Acid, Vitamin B2 and 2, 5-Dichloroaniline). The limit of detections (LoD) of α-lactose, benzoic acid, vitamin B2 and 2,5-dichloroanline are 8.61 mg/mL, 6.96 mg/mL, 7.54 mg/mL and 8.35 mg/mL, respectively. This work opens the way to multiple THz fingerprint trace detection and provides potential platforms for specific biomarker recognition in biomedical and environment applications.

2. Structure design and theoretical analysis

2.1. N- concentric rings structures

The N-order concentric rings structures are illustrated in the column 1 of Fig. 1, where the periodicity of a unit cell is 120 μm and N(1–5) represents the number of concentric rings. For N = 1, the radius of the inner ring is 50 μm and the width of the rings is 5 μm. For N = 5, the radiuses of the inner rings are 50 μm, 40 μm, 30 μm, 20 μm and 10 μm, respectively. Fig. 1 (column 2) shows the simulation results of transmission spectra of corresponding N-order structure by utilizing the commercial software Computer Simulation Technology (CST) Microwaves Studio. General speaking, there are N modes (transmission dips) for N-order concentric rings structure. Fig. 1 (column 3) shows the electric-field distributions at resonance frequencies points for different N. The electric field distributions indicated that the excited modes are almost the eigen dipole modes corresponding to different diameter rings in N-order concentric rings structure, except that (4, 4) (5, 4) and (5, 5) modes show hybrid modes. For instance, (5, 4) hybrid mode coms from the interaction between higher order mode(hexapole) on 50 μm radius ring and dipole mode on 20 μm radius ring. The resonance frequencies at different N are listed in Table 1. When N increases, the resonance frequency of dipole mode in the same radius ring is somewhat redshift due to near field capacitive coupling between nearby concentric rings. So the equivalent circuit model [21] for each N is built to investigate and design accurate reconfigurable multiple resonance position, as show in column 4 in Fig. 1. In equivalent circuit model, a ring can be presented as a Inductor-Capacitor (LC) resonance circuit. Between rings there exists coupling capacities C_M, and a parameter changing is equivalent to changing the LC parameters in the equivalent circuit, causing the shift of resonance frequency. If the designed resonance frequencies of the proposed metasensor perfectly matches the fingerprint absorption peak of the chemical substances, a multiple-chemical substances fingerprint trace detection can be realized.

2.2. Designed metasensor for simultaneously detecting 4 chemical substances

Fig. 2(a) illustrates the designed 5-order concentric rings structures for simultaneously detecting 4 chemicals (α-Lactose, Benzoic Acid, Vitamin B2 and 2,5-Dichloroaniline). The substrate is made of polyimide with 70 μm-thick. The periodicity of the unit structure is 120 μm in both X and Y directions. The inner radius of each concentric ring is $R_1 = 14$ μm, $R_2 = 23$ μm, $R_3 = 32$ μm, $R_4 = 40$ μm and $R_5 = 48$ μm with the width w = 5 μm, as shown in Fig. 2(b). The conductivity of the gold is 4.561×10^7 $S/$m and the dielectric constant of the polyimide is $3.5 + 0.001$i. The photograph of the fabricated wafer chip includes 4 identical multiple fingerprint metasensor, as illustrated in Fig. 2(c). The simulated transmission spectra of the designed structure are shown in Fig. 2(d). There are 4 significant resonant frequency dips ($f_1 = 0.62$ THz, $f_2 = 0.77$ THz, $f_3 = 0.98$ THz, $f_4 = 1.32$ THz) in the range from 0.4 THz to 1.4 THz. The simulated electric field distributions at 0.62 THz, 0.77 THz, 0.98 THz, and 1.32 THz are shown in Fig. 2(e)–(h), which corresponding to dipole modes for R_5, R_4, R_3, and R_2 rings, respectively. Moreover, the perfect dipole modes can be achieved by optimize parameters of 5-order concentric rings structures. The discussion of transmission spectra with different structure's parameters, such as periodicity of the unit cell (P), the radius deviation of each inner ring (δ) and the width of ring (w), are illustrated in Supplementary Material Section 1.

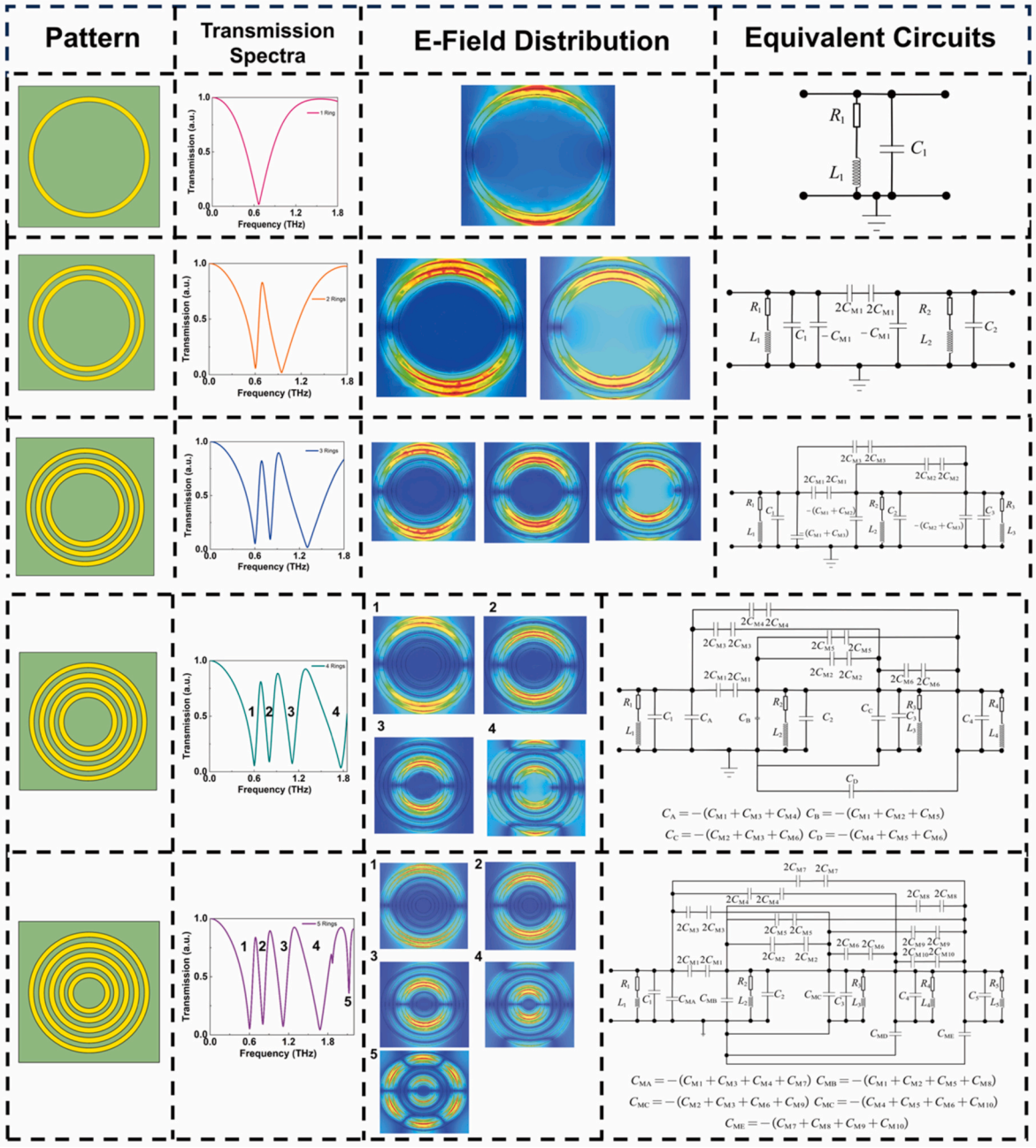

Fig. 1. N-order (N from 1 to 5) concentric ring structure patterns(column 1), transmission spectra(column 2), electric field distribution at each resonant frequency (column 3) and the equivalent circuit models (column 4).

Table 1
The resonant frequencies of N-order concentric structure.

M / *N*	Resonant Frequency (THz)				
	1	2	3	4	5
1	0.668	NA	NA	NA	NA
2	0.604	0.946	NA	NA	NA
3	0.602	0.808	1.306	NA	NA
4	0.602	0.804	1.112	1.766	NA
5	0.6	0.804	1.116	1.676	2.116

2.3. Influence of real and imaginary parts of permittivity on AIT effect of 5-ring structure

To obtain optical properties and the absorption features of chemical substances, Lorentz dispersion model can be utilized and expressed as:

$$\tilde{\varepsilon}(\omega) = \sum_{j=1}^{m} \frac{f_j \omega_{pj}^2}{\left(\omega_{0j}^2 - \omega^2\right) + i\gamma_j \omega} \tag{1}$$

where m is the number of oscillators with the resonance frequency ω_{0j}; ω_p is the plasma frequency; F_j is the oscillator strength; γ is the damping constant, i.e. the full width half maximum. The real and imaginary part of chemical substance permittivity can be expressed as [22–24]:

$$\varepsilon_{real}(\omega) = \varepsilon_\infty + \sum_{j=1}^{m} \frac{f_j \omega_{pj}^2 \left(\omega_0^2 - \omega^2\right)}{\left(\omega_{0j}^2 - \omega^2\right)^2 + \gamma_j^2 \omega^2} \tag{2}$$

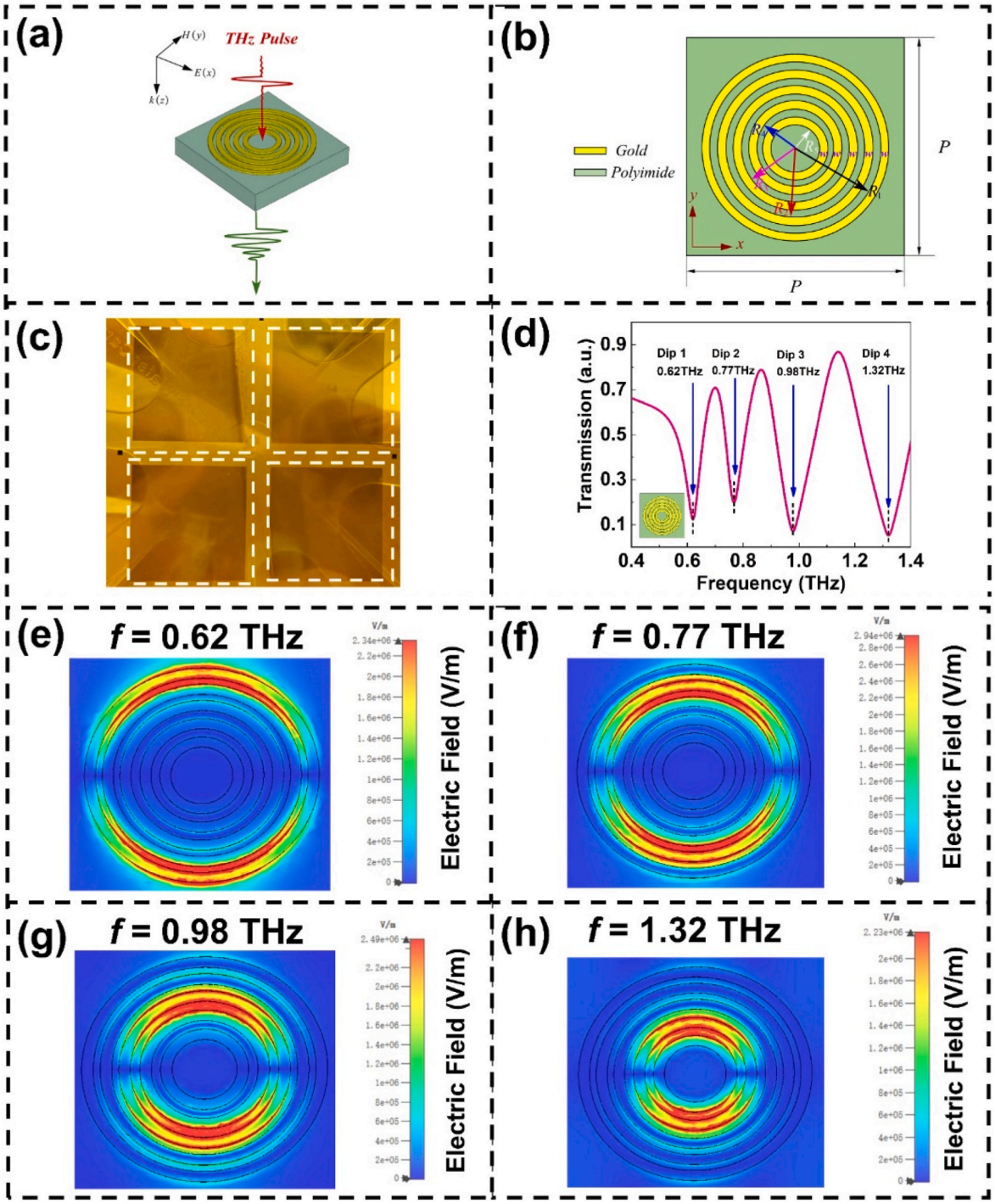

Fig. 2. (a) Three-dimension diagram of THz multiple fingerprint metasensor (b) diagram of 5-order concentric rings structures (c) the fabricated wafer chip includes 4 identical multiple fingerprint metasensors. (d) Transmission spectra of the designed structure. (e)–(h) Simulated electric field distributions at 0.62 THz, 0.77 THz, 0.98 THz, and 1.32 THz, respectively.

$$\varepsilon_{imaginary}(\omega) = \sum_{j=1}^{m} \frac{f_j \omega_{pj}^2 \gamma_j \omega}{\left(\omega_{0j}^2 - \omega^2\right)^2 + \gamma_j^2 \omega^2} \tag{3}$$

where ε_∞ denotes the off-resonance background permittivity of the chemical substances, and the complex refraction index can be expressed by $n + ik$. If the N-order concentric rings metasensor could be controlled such that the broadband dipole resonances in the N-order concentric rings metasensors interact with the narrowband fingerprint absorption spectra of the 4 selected samples with tiny quantity to interfere destructively, the AIT effect can be observed through the transmission spectra that a clear 'W' shape lines occurs due to narrowband transparency peak near the resonance frequency, which means the designed sensor is specific to the chemical substances [25,18].

2.3.1. *The influence of the real part of permittivity*

Fig. 3(a) illustrates the transmission spectra for different thicknesses of chemical substances. Chemical substances thickness with respect to four resonance frequency shifts ($\Delta f_1 \sim \Delta f_4$) of the metasensor was investigated in Fig. 3(b). The real part of permittivity of four chemical

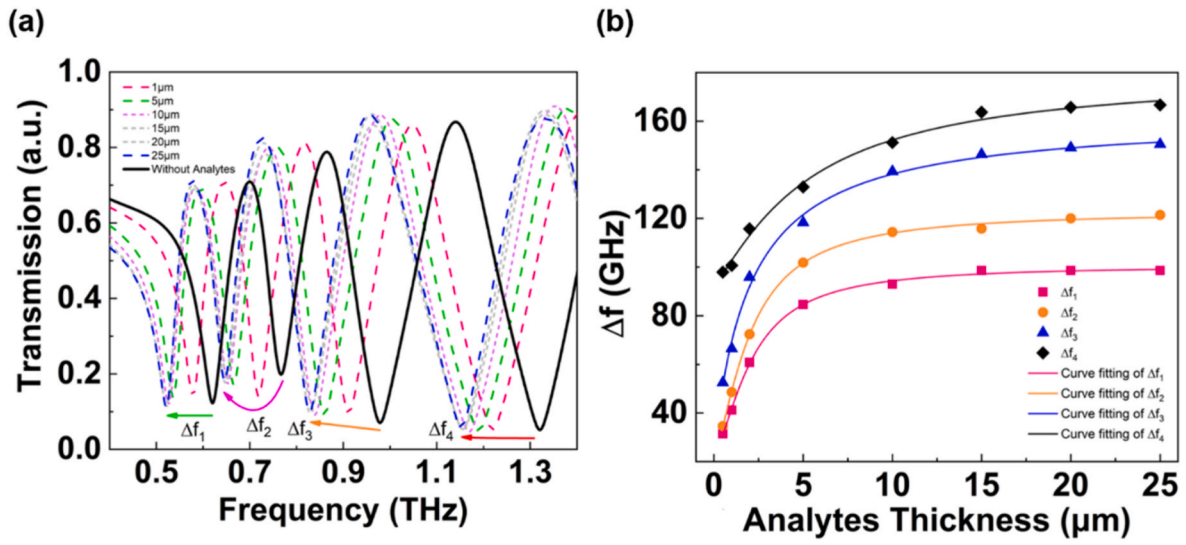

Fig. 3. (a) Transmission spectra of different thicknesses of chemical substances, (b) frequency shifts of four dips with respect to different thicknesses of chemical substances.

substances is set to 3.14 [26,27]. We observe that the four resonance frequency shifts ($\Delta f_1 \sim \Delta f_4$) increase exponentially with the increasing chemical substances thickness and eventually saturate at about 10 μm thickness due to the fact that the confinement length of electric field is up to 10 μm above the metasensor layer. The cutoff $\Delta f_1 \sim \Delta f_4$ are 0.098 THz, 0.12 THz, 0.15 THz, and 0.167 THz for chemical substances α-lactose, benzoic acid, vitamin B2 and 2, 5-dichloroanline, respectively. Since the selected fingerprint frequencies of absorption spectra are 0.53 THz (α-Lactose) [28–30], 0.64 THz (Benzoic Acid) [31,32], 0.82 THz (Vitamin B2) [33] and 1.17 THz (2,5-Dichloroaniline) [34] (experiment absorption lines of the chemical substances have been plotted in Supplementary Material Section 2), the designed multiple fingerprint metasensor should consider such frequency shifts owing to real part permittivity and the four dipole resonance frequencies are designed at 0.62 THz, 0.77 THz, 0.98 THz, and 1.32 THz, as described in section 2.2.

2.3.2. *The influence of the imaginary part of permittivity*

By utilizing Lorentz dispersion model in Eq. (3), the imaginary parts

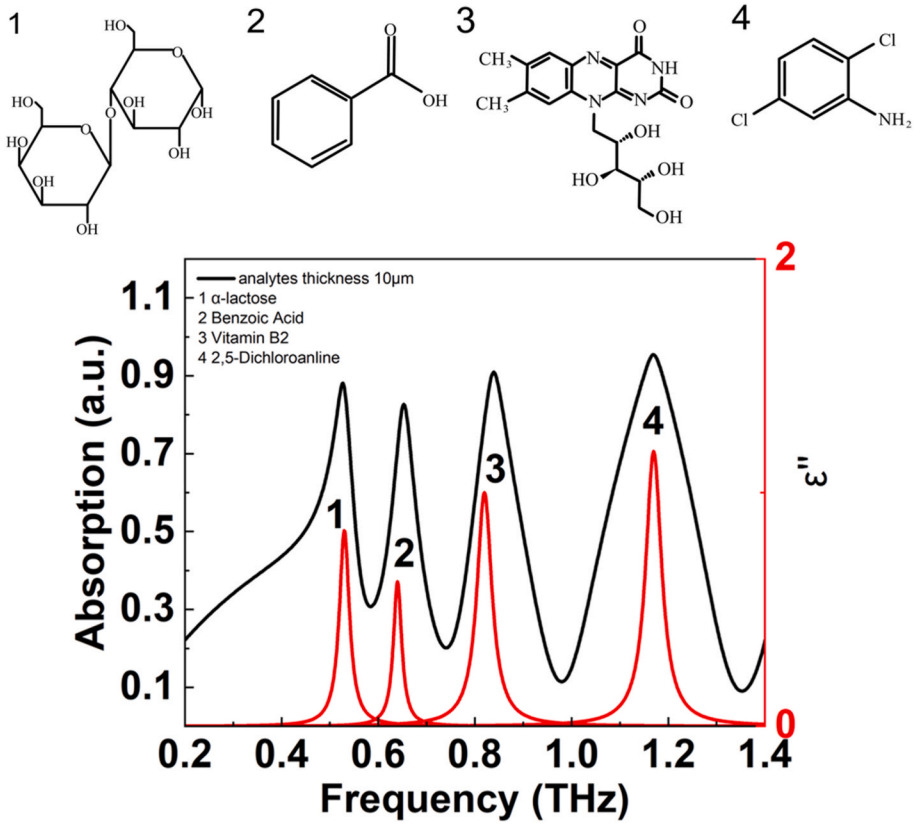

Fig. 4. The comparison of 4 chemical substances' imaginary part of permittivity (red line) and the absorption spectra of metasensor which is covered by 10 μm-thick chemical substances (black line). On the top: chemical structure of α-lactose, benzoic acid, Vitamin B2 and 2,5-dichloroanline.

of permittivity of four chemical substances are illustrated in Fig. 4 (red lines). We also plotted the absorption spectrum of proposed fingerprint metasensor considering frequency shifts for 10 μm-thick chemical substances (black line). The broadband dipole resonances in the 5-order concentric rings metasensors and the narrowband fingerprint absorption spectra of the 4 selected chemical substances can be clearly observed in Fig. 4. The top inset of Fig. 4 also illustrates the molecule structures of four different chemical substances.

Next, we will discuss the AIT effects in each dipole resonances. Fig. 5 (a) shows that the amplitude transmission spectra of designed 5-order concentric rings structure coated with several concentrations of α-lactose. The relationship between thickness and concentration can be found in Supplementary Material section 3. There is a vibrational transmission peak located at 0.53 THz, which agrees well with bulky pellet samples (See Supplementary Material 2 Fig. S2). When the concentration of chemical substances is 5 mg/mL, the AIT effects on the fingerprint dips of α-lactose are not obvious. With the increase of the concentration of chemical substances (20 mg/mL), the four transparency peaks from AIT at fingerprint dip can be clearly found due to destructive interference between the broadband oscillations in the 5-order concentric rings plasmonic metasensor and the narrowband oscillations of the α-lactose, while resonances dips at 0.64 THz, 0.82 THz and 1.17 THz are almost unchanged. It indicates that the transmission spectrum of dip1 of the designed 5-order concentric rings structure is only controlled by α-lactose. Similar phenomena can also be found for chemical substances of benzoic acid, Vitamin B2 and 2,5-dichloroanline as shown in Fig. 5(b)–(d). For instance, the AIT effect at 0.64 THz can be clearly observed when only benzoic acid is coated on the metasensor, while the transmission dips at 0.53 THz, 0.98 THz and 1.17 THz still exist with the concentration of 20 mg/mL (Fig. 5(b)). In addition, in

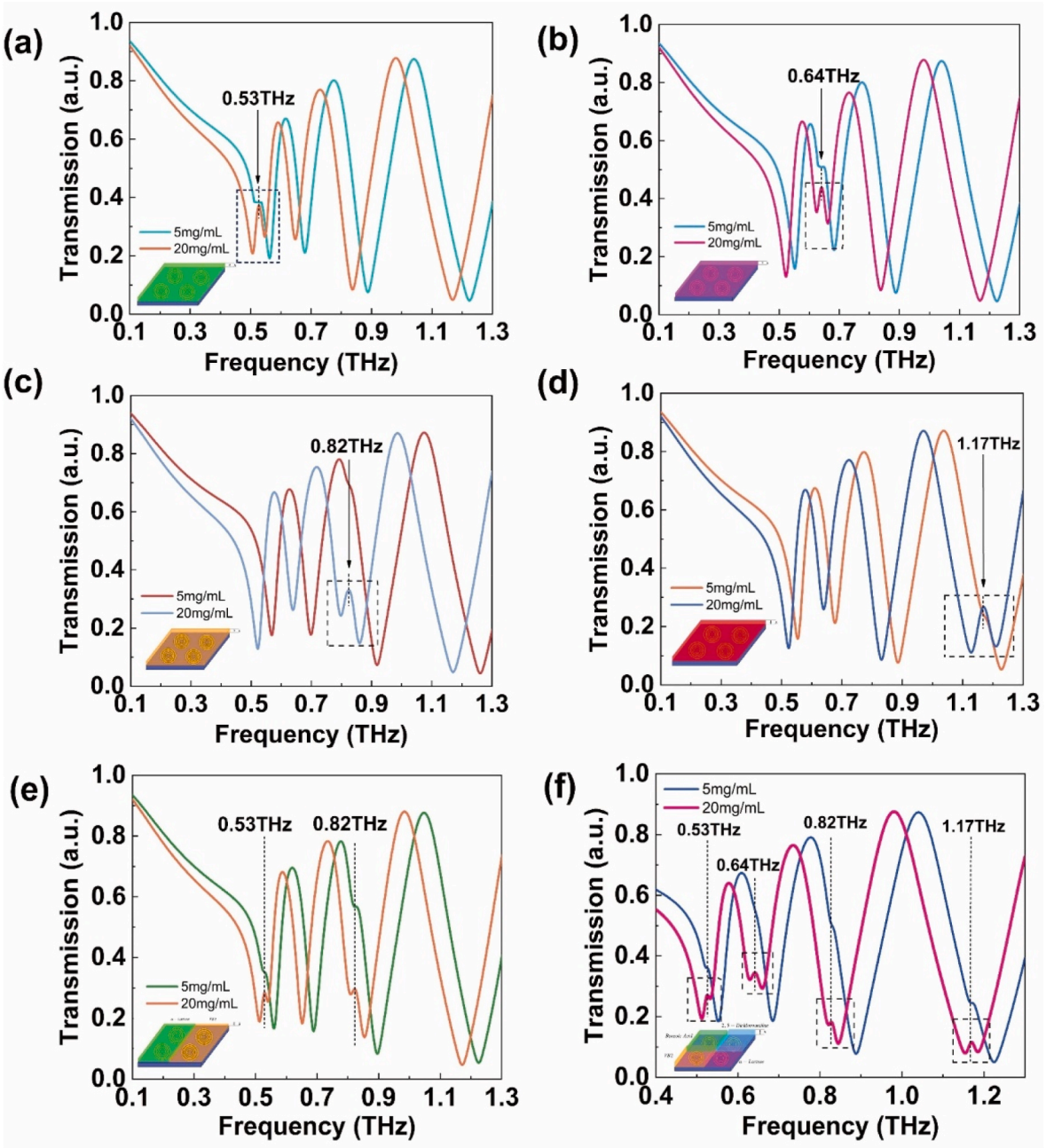

Fig. 5. Simulated transmission spectra of: (a) α-lactose, (b) Benzoic acid, (c) Vitamin B2, (d) 2,5-dichloroanline (e) 1:1 mixture of α-lactose and VB2 and (f) identical ratio mixture of four chemicals at the same time, with concentrations of 5 mg/mL and 20 mg/ml.

Fig. 5(e), transmission spectrum for mixture of α-lactose and vitamin B2 (1:1) with 20 mg/mL concentration on the metasensor indicates that AIT can be found at 0.53 THz and 0.82 THz simultaneously. Similarly, the mixture of benzoic acid and 2, 5-Dichloroaniline (1:1) can also be clearly identified from the transmission spectra (not shown here). So we can identify two chemical substances at the same time. Fig. 5(f) presents the simulated results of four chemicals at the same time. With the increase of the concentration of chemical substances (20 mg/mL), the four transparency peaks from AIT at each fingerprint dip can be simultaneously found. The above results means that our designed 5-order concentric rings structure is a unique platform for recognizing single and mixed molecular fingerprints with low concentration.

3. Experiment results

The specific experiment steps are shown in Fig. 6. The α-Lactose used in the experiment was purchased from the Shanpu, Shanghai, China, and the other chemicals were purchased from Aladdin, Shanghai. The various concentrations of 4 chemical substances (α-lactose, benzoic acid, Vitamin B2 and 2,5-dichloroanline) solutions were prepared by diluting chemicals solution with deionized water in different solutions. After the solutions were settled, they were put into a vortex mixer with the rotation speed of 2800 rpm to shake the solution for 15 s to obtain the sample solution in suspension. Before measurements, a droplet (10 μL) of chemical solution was dripped onto the surface of the metasensor. And then metasensor with the solution was heated at a temperature of 100 °C on a hotplate for 20 min to accelerate the crystallization process. Next, the metasensor with chemical substances were measured by commercial THz-TDS (TAS7400, Advantest Ltd., Tokyo, Japan). The effective frequency range of the system was 0.2–3.0 THz with the signal dynamic range 60 dB and the spectral resolution 7.6 GHz. The measurement for one chip was repeated four times.

We firstly measured time-domain waveform of THz wave passing through freespace(reference) and metasensor (sample), as shown in Fig. 7(a). Long and pronounced damping oscillation can be observed when THz wave passes through metasensor (red line) in Fig. 7(a). We also fabricated the 5-order concentric rings structure in four different area (P1–P4) on one wafer. The transmission spectrum of the area P1 was plotted in Fig. 7(b). The resonance frequencies of the 4 transmission dips are 0.617 THz,0.78 THz, 1.017 THz and 1.35 THz, the results are close to the simulation ($f_1 = 0.62$ THz, $f_2 = 0.77$ THz, $f_3 = 0.98$ THz, $f_4 = 1.32$ THz). The experimental spectra of areas P2–P4 were also shown in Fig. S4 in Supplementary Material Section 4. The curves are almost the same due to little fabrication error between four different fabrication areas with same pattern. The replication of transmission spectra is excellent.

We also presented the blank response of the proposed metasensor together with responses to different chemical substances in the experimental results, as shown in Fig. 8. The experimental transmission spectra of bare chip as well as 4 different α-lactose concentrations (5, 20, 30, 40 mg/mL) were shown in Fig. 8(a). When 5 mg/mL α-lactose was covered on the metasensor, the AIT effect wasn't observed in the redshifted lowest resonance frequency dip. As the concentration increases to achieve 20 mg/mL (10 μm), a transparency peak due to AIT at 0.53 THz was observed. Such transparency peak can also be found at concentrations of 30 and 40 mg/mL. While dips at 0.64 THz, 0.82 THz and 1.17 THz remain invariable. As the concentration is greater than 20 mg/mL, the transparency peak position due to AIT shows little redshift effect owing to the fact that the concentration (thickness) of α-lactose is within the saturation region (Fig. 3(b)). Similarly, the AIT effect is clearly found at the corresponding absorption peak of other three chemical substances (20, 30, 40 mg/mL), as illustrated in Fig. 8(b)~(d). Our designed 5-order concentric rings structure can specifically detect α-lactose, benzoic acid, vitamin B2 and 2,5-dichloroanline. Experimental results agree well with the simulated ones.

According to the concentration range of the four chemicals (α-lactose, benzoic acid, vitamin B2 and 2, 5-dichloroanline), we tested samples with different concentrations for the quantitative calibration. The amplitude difference (ΔAmp) is defined as the minimum differences between maximum to minimum transmission amplitude around the resonance (See Supplementary Material Section 5). With increase of C_A from 5 to 40 mg/mL, the amplitude differences of AIT increase linearly, as shown in Fig. 8(a)–(d). The corresponding functions of the regression lines in each fingerprint frequencies are as follows:

$$\Delta Amp_{\text{α-Lactose}} = 2.11\times10^{-3} \times C_A\text{-}0.01164, \text{SD} = 0.00218, R^2 = 0.996 \quad (4)$$

$$\Delta Amp_{\text{Benzoic Acid}} = 2.08\times10^{-3} \times C_A\text{-}0.01074, \text{SD} = 0.00125, R^2 = 0.998 \quad (5)$$

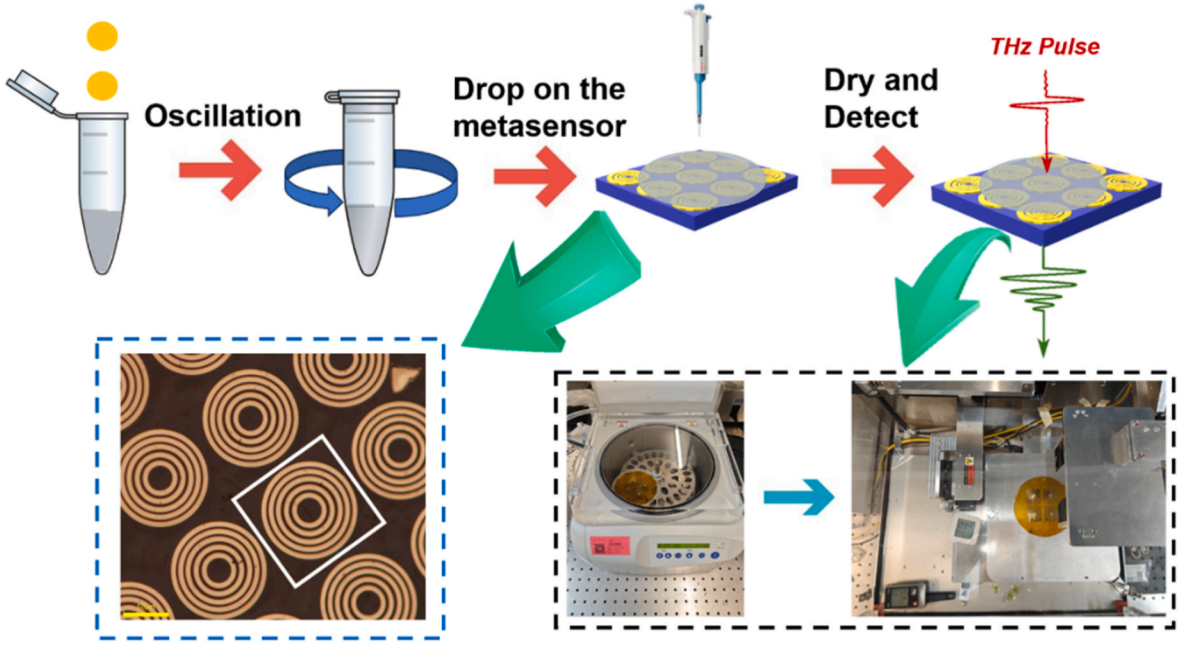

Fig. 6. Top: specific experiment scheme; Bottom: optical microscopy image of the fabricated metasensor (left), chip heating image (middle) and experimental setup by using THz-TDS (right).

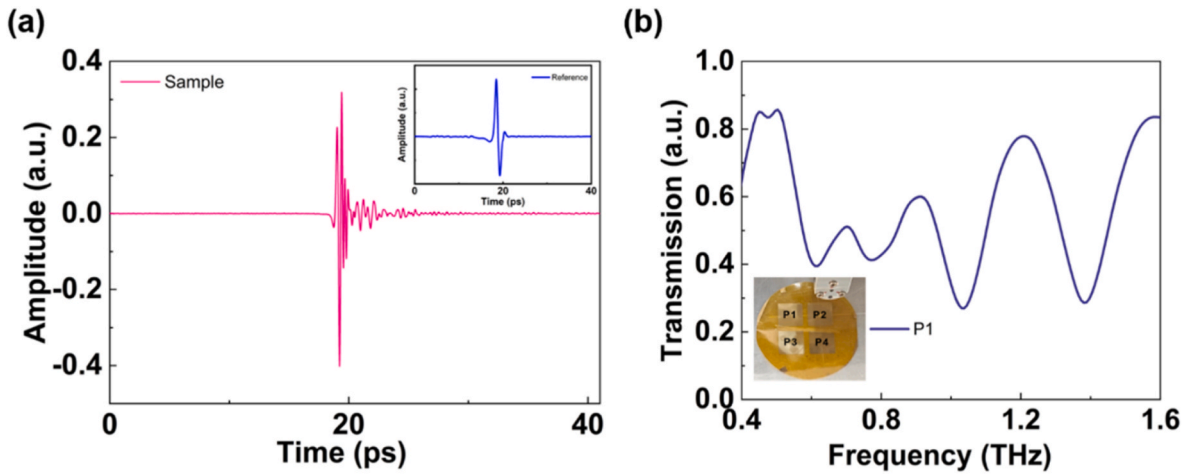

Fig. 7. Experiment results of: (a) time-domain signals, (b) transmission spectrum of the metasensor pattern area P1.

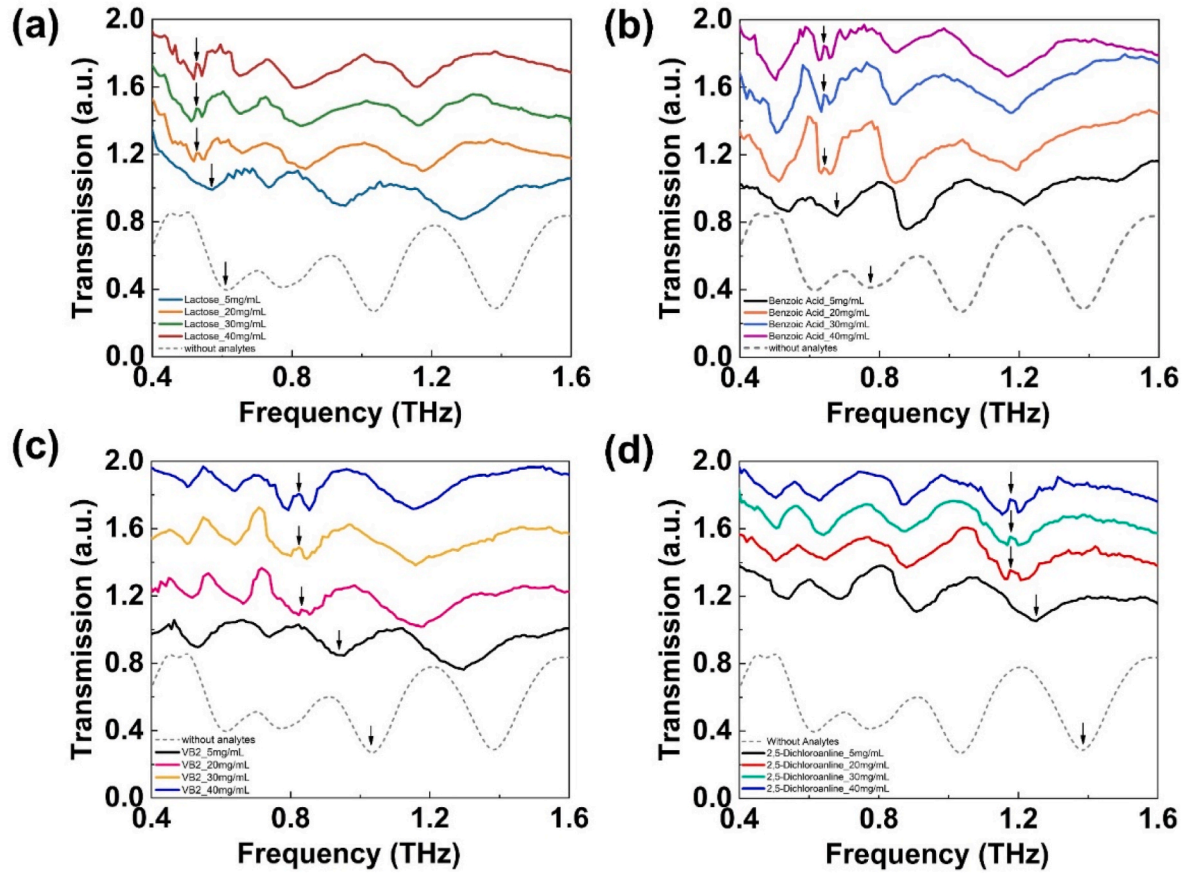

Fig. 8. Experiment transmission spectra of four chemical substances (a) α-lactose, (b) benzoic acid, (c) vitamin B2 and (d) 2,5-dichloroanline with different concentrations (5, 20, 30, 40 mg/mL). Each curve shifted (+0.4) toward y axis in order for clarity. The blank response has also been plotted in each graph.

$$\Delta Amp_{\mathrm{VB2}} = 2.11\times10^{-3} \times C_A\text{-}0.01135, \mathrm{SD} = 0.00152, R^2 = 0.998 \quad (6)$$

$$\Delta Amp_{\mathrm{Dichloroanline}} = 2.19\times10^{-3} \times C_A\text{-}0.0122, \mathrm{SD} = 0.00203, R^2 = 0.996 \quad (7)$$

where C_A is the concentration of four chemicals (mg/mL), SD is the standard deviation of ΔAmp (arb. unit), and R^2 is the correlation coefficient of linear fitting. All R^2 in Fig. 8(a)~(d) are greater than 0.995, indicating that these four regression lines nearly perfectly fits the experimental data. The lowest detection limit (LoD) of our method can be calculated according to 3 s/m method:

$$\mathrm{LoD} = 3\times\mathrm{SD} / k \quad (8)$$

where k is the slope of the linear fitting. LoD is 8.61 mg/mL (α-lactose), 6.96 mg/mL (benzoic acid), 7.54 mg/mL (vitamin B2) and 8.35 mg/mL (2,5-dichloroanline) according to Fig. 9(a)–(d) and Eq. (8).

Furthermore, we analyzed the specific detection for proposed metasensor. The results are from detection of four chemicals individually on four different metasensors (P1–P4). Experiment was done for each chemical substance with 10 different concentrations and repeated for

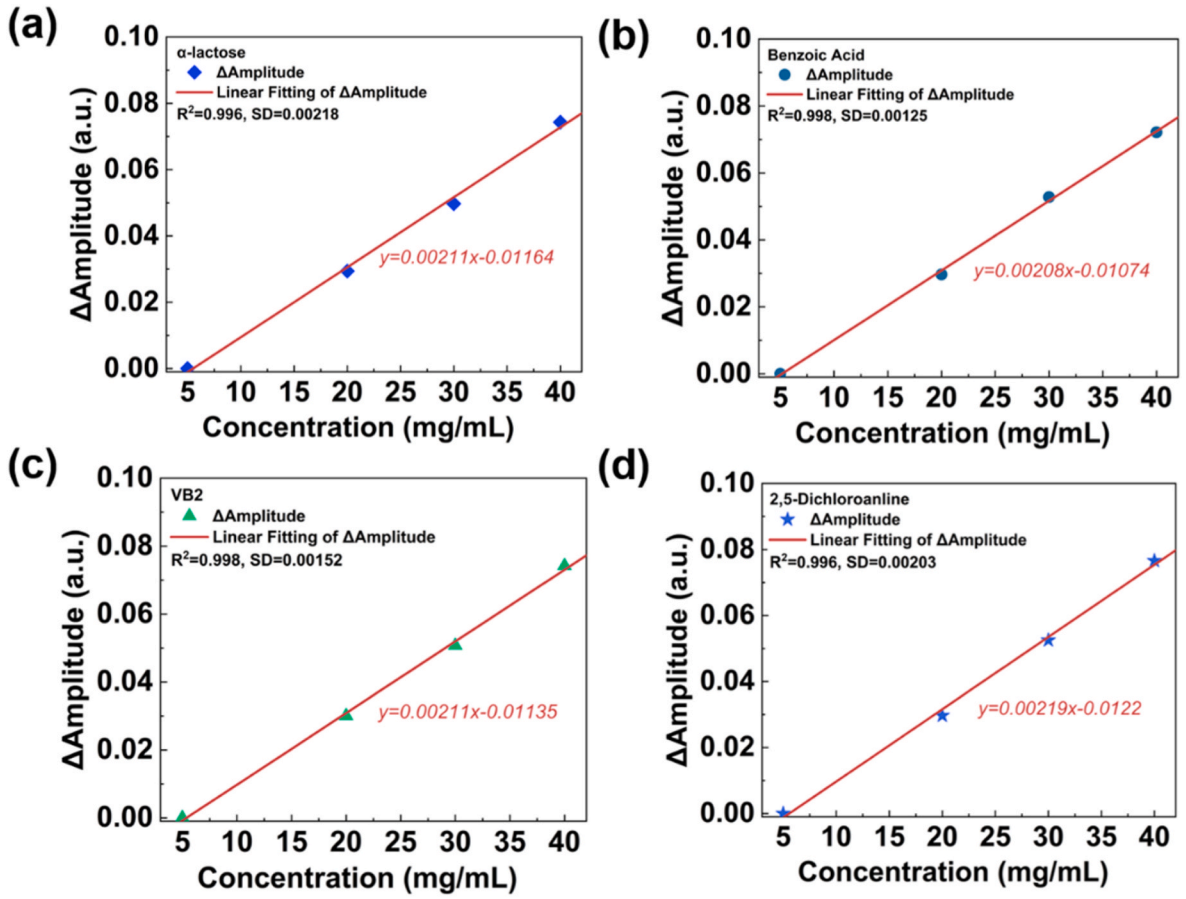

Fig. 9. ΔAmp of four chemicals with respect to concentration for (a) α-lactose (b) benzoic acid (c) vitamin B2 (d) 2,5-dichloroanline.

four times. The results from Fig. 10 reveal that the transparency peak frequencies of the α-lactose (blue triangles) locate at the lowest frequency range. And the specific frequencies of 2,5-dichloroanline(green rectangular) are at the highest frequency range. The specific frequencies of benzoic acid (red circles) are lower than vitamin B2 (orange pentagrams), and both of them embedded between α-lactose and 2,5-dichloroanline. In this case, the whole spectrum is divided into four regions: region I is from 0.52 to 0.55 THz for α-lactose identification range; region II is from 0.62 to 0.66 THz for benzoic acid identification range; region III is from 0.815 to 0.825 THz for vitamin B2 identification range; region IV is from 1.158 to 1.175 THz for 2,5-dichloroanline identification range. By using the one-way analysis of variance (ANOVA) method35, the possibility of recognition error by THz metasensor detection is lower than 0.001. Four chemical substances can be distinguished successfully. The proposed THz metasensor has the advantages of better differentiation, smaller error and higher discrimination.

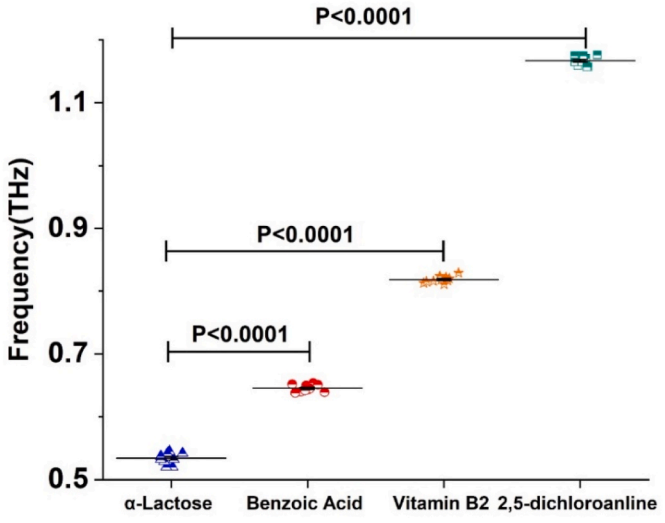

Fig. 10. ANOVA analysis of THz detection results.

We also measured transmission spectra of four chemicals with concentrations 5 mg/mL and 20 mg/mL at the same time, as presented in Fig. 11(a). The AIT effects can be observed with the concentrations of 20 mg/mL while they are disappear at 5 mg/mL. The experimental results fit well with the simulation in Fig. 5(f). The ANOVA method was also used to analyze results of four chemicals covered on single metasensor at the same time, as shown in Fig. 11(b). The possibilities of recognition error for these chemicals are all lower than 0.001. It means that four chemicals can be successfully distinguished from their mixture simultaneously.

4. Discussion and conclusion

Table 2 compared performances of different THz metasensor, especially AIT metasensor. There are two kinds of principles in THz sensing: refractive index sensing and AIT detection. As for the former one, frequency dip deviation in the transmission spectra can be observed due to the change of the chemical substances' permittivity. However, the specific identification of THz fingerprint spectrum of chemical substances is ignored [36–38]. For the fingerprint sensing based on AIT detection, previous works can specifically detect only one chemical substance. They cannot deal with multiple chemical substances and their mixture. Furthermore, the obvious resonance frequency deviation of the

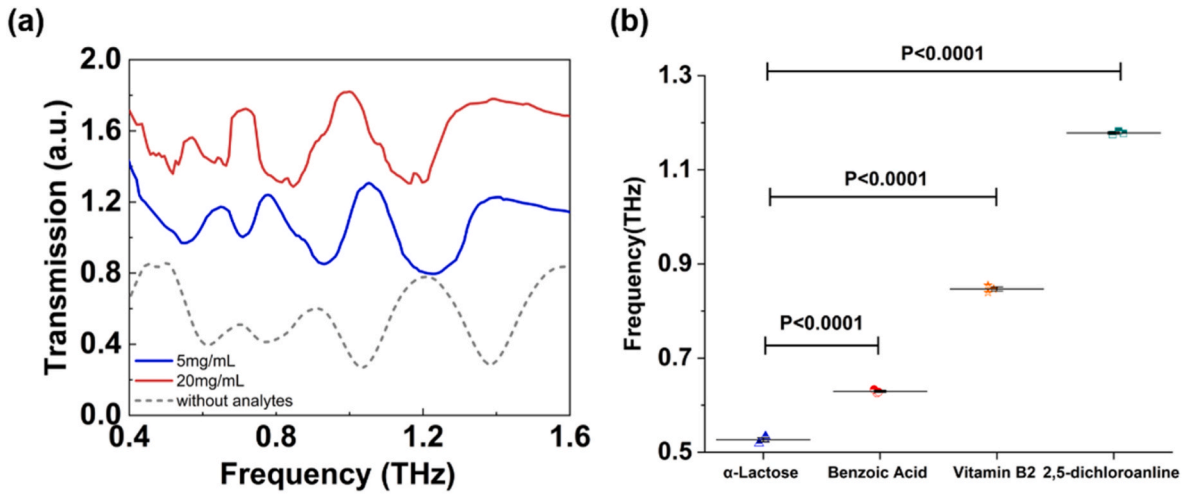

Fig. 11. (a) The experimented transmission spectra of four chemicals at the same time (b) ANOVA analysis of THz detection results with four chemicals covered on the metasensor at the same time.

Table 2
Comparison with THz refractive index and AIT metasensors.

Work	Structures	Substances	number of substances	Reconfiguration	Mixture Detection	Principles
Ref [16]	Concentric Rings	Oral Cancer Cell (SCC4)	1	NA	×	Refractive index sensing
Ref [17]	SRRs	VOCs	1	NA	×	Refractive index sensing
Ref [9]	Comb-shaped waveguide	α-lactose	1	Changing the geometrical parameters	×	AIT
Ref [20]	InSb coupled rod	α-lactose	1	Temperature & Static magnetic fields	×	AIT
Ref [19]	SRRs	α-lactose	1	NA	×	AIT
Ref [18]	SRRs	L-tartaric	1	NA	×	AIT
Ref [39]	Cross-slot array	α-lactose	1	Changing the geometrical parameters	×	AIT
Ref [40]	SRRs array	L-glutamate	1	Changing the geometrical parameters	×	AIT
Our work	N-order Concentric Rings	α-lactose, benzoic acid, VB2 and 2,5-dichloroanline.	4	Altering parameters of structure and the amount of rings	✓	AIT

metasensor caused by the real part of chemical substances' permittivity cannot be discussed and compensated in more details. In our work, the proposed N-order concentric rings plasmonic structure can achieve specific fingerprint detection for multiple chemical substance by considering resonance frequency deviation due to the real parts of permittivity, exhibiting good multiple AIT performance.

The AIT can achieve THz trace molecular fingerprint sensing. The most intriguing characteristic of AIT is that the transmission peak, in the combined metasensor device with chemical substance system, appears at the spectral position where the bare chemical substance presents resonant absorption. However, there still exists some limitations. AIT can't be excited for the coherent coupling of a narrowband mode of the metasensor to a broadband absorption line/resonance of chemical substance. More recently, multiplexing array has also been used to trace molecular fingerprint sensing due to strong light–matter interaction between a series of narrowband resonant peaks of metasensors with broadband mode resonance of chemical substance. Combing the AIT effect with multiplexing may improve such limitation for trace THz molecular fingerprint sensing [39]. In potential future research, three directions may be paid more attentions: 1) extension of this work to other practical implications in environmental protection and medicines identification [41,42]. 2) improvement of robustness of AIT identification by using metasensor array [39,40]; 3) development of platform which can achieve enhanced trace fingerprint detection that can deal with both broadband and narrowband absorption line/resonance of chemical substance [39].

In summary, the N-order concentric rings plasmonic metasensor has been investigated for simultaneous multiple THz fingerprint detection. We have observed different dipole resonance mode due to different diameters of the concentric rings. We also established circuit models to explain the principle of the near field weak interaction between concentric rings. For multiple fingerprint detection, we selected N as 5 and altered the parameters to excite four dipole modes. To fit perfectly with the fingerprint absorption spectra of four chemical substances (α-Lactose, Benzoic Acid, Vitamin B2 and 2,5-Dichloroaniline) and their mixture, the metasensor was carefully designed to compensate the frequency-shift caused by the real part of the chemical substances' permittivity. Simulation and experimental results prove that the metasensor can specifically and simultaneously detect 4 chemical substances. Our work creates a new avenue in THz fingerprint trace detection of multiple chemical substances and mixed chemical substances and provides potential platforms for specific biomarker recognition in practical biomedical and environment applications. For instance, many industrial solid wastes, such as pyrazinamide, benazepril, cefprozil, and bisphenol, have shown significant THz fingerprint features [41]. By using this method and combing with chemometrics, we can quantitatively analyze

and identify industrial solid wastes in actual mixtures. Our new method can also be utilized for the rapid qualitative and quantitative identification of medicines which also have significant THz fingerprint features such as Caffeine, Carnitine, etc [39,42].

CRediT authorship contribution statement

Lihao Huang: Data curation, Formal analysis, Investigation, Software, Writing – original draft. **Hongyan Cao:** Data curation, Formal analysis, Investigation, Methodology, Software, Validation, Writing – original draft. **Lin Chen:** Conceptualization, Data curation, Formal analysis, Funding acquisition, Investigation, Methodology, Project administration, Resources, Supervision, Validation, Writing – review & editing. **Yi Ma:** Data curation, Formal analysis, Methodology, Software, Writing – review & editing. **Yihan Yang:** Data curation, Writing – review & editing. **Xiaoyang Liu:** Data curation, Methodology, Software, Writing – review & editing. **Wenqi Wang:** Data curation, Investigation. **Yiming Zhu:** Funding acquisition, Writing – review & editing. **Songlin Zhuang:** Funding acquisition, Supervision, Writing – review & editing.

Declaration of competing interest

The authors declare that they have no known competing financial interests or personal relationships that could have appeared to influence the work reported in this paper.

Data availability

Data will be made available on request.

Acknowledgement

This work was supported in part by Basic Science Center Project of the National Natural Science Foundation of China [Grant No. 61988102]; National Natural Science Foundation of China [Grant No. 62275157]; Shanghai Shuguang Program [Grant No. 18SG44]; 111 Project [Grant No. D18014].

Appendix A. Supplementary data

Supplementary data to this article can be found online at https://doi.org/10.1016/j.talanta.2023.125481.

References

[1] J. Qin, Y. Ying, L. Xie, The detection of agricultural products and food using terahertz spectroscopy: a review, Appl. Spectrosc. Rev. 48 (6) (2013) 439–457.
[2] S. Li, Y. Tian, P. Jiang, Y. Lin, X. Liu, H. Yang, Recent advances in the application of metabolomics for food safety control and food quality analyses, Crit. Rev. Food Sci. Nutr. 61 (9) (2021) 1448–1469.
[3] I. Timofeeva, D. Kanashina, K. Stepanova, A. Bulatov, A simple and highly-available microextraction of benzoic and sorbic acids in beverages and soy sauce samples for high performance liquid chromatography with ultraviolet detection, J. Chromatogr. A 1588 (2019) 1–7.
[4] C.M. Phechkrajang, S. Yooyong, Fast and simple method for semiquantitative determination of calcium propionate in bread samples, J. Food Drug Anal. 25 (2) (2017) 254–259.
[5] J.S. So, S.B. Lee, J.H. Lee, H.S. Nam, J.K. Lee, Simultaneous determination of dehydroacetic acid, benzoic acid, sorbic acid, methylparaben and ethylparaben in foods by high-performance liquid chromatography, Food Sci. Biotechnol. 32 (9) (2023) 1173–1183.
[6] R. Lapchareonsuk, P. Sirisomboon, Sensory quality evaluation of rice using visible and shortwave near-infrared spectroscopy, Int. J. Food Prop. 18 (5) (2015) 1128–1138.
[7] L. Sun, G. Hui, S. Gao, J. Liu, L. Wang, C. Dai, Prediction of benzoyl peroxide in flour using near infrared spectroscopy technique, Int. J. Food Prop. 19 (5) (2016) 1115–1126.
[8] X. Fu, J. Chen, F. Fu, C. Wu, Discrimination of talcum powder and benzoyl peroxide in wheat flour by near-infrared hyperspectral imaging, Biosyst. Eng. 190 (2020) 120–130.
[9] X. Shi, J. Qin, Z. Han, Enhanced terahertz sensing with a coupled comb-shaped spoof surface plasmon waveguide, Opt Express 25 (1) (2017) 278.
[10] H.-B. Liu, Y. Chen, G.J. Bastiaans, X.-C. Zhang, Detection and identification of explosive RDX by THz diffuse reflection spectroscopy, Opt Express 14 (1) (2006) 415.
[11] Y. Ueno, K. Ajito, N. Kukutsu, E. Tamechika, Quantitative analysis of amino acids in dietary supplements using terahertz time-domain spectroscopy, Anal. Sci. 27 (4) (2011) 351–356.
[12] X. Zang, B. Yao, L. Chen, J. Xie, X. Guo, A.V. Balakin, A.P. Shkurinov, S. Zhuang, Metasurfaces for manipulating terahertz waves, Light Adv. Manuf. 2 (2) (2021) 148.
[13] Y. Zhu, X. Zang, H. Chi, Y. Zhou, Y. Zhu, S. Zhuang, Metasurfaces designed by a bidirectional deep neural network and iterative algorithm for generating quantitative field distributions, Light Adv. Manuf. 4 (2) (2023) 1.
[14] H. Zhou, C. Yang, D. Hu, D. Li, X. Hui, F. Zhang, M. Chen, X. Mu, Terahertz biosensing based on bi-layer metamaterial absorbers toward ultra-high sensitivity and simple fabrication, Appl. Phys. Lett. 115 (14) (2019), 143507.
[15] R. Melik, E. Unal, N.K. Perkgoz, C. Puttlitz, H.V. Demir, Metamaterial based telemetric strain sensing in different materials, Opt Express 18 (5) (2010) 5000.
[16] C. Zhang, L. Liang, L. Ding, B. Jin, Y. Hou, C. Li, L. Jiang, W. Liu, W. Hu, Y. Lu, L. Kang, W. Xu, J. Chen, P. Wu, Label-free measurements on cell apoptosis using a terahertz metamaterial-based biosensor, Appl. Phys. Lett. 108 (24) (2016), 241105.
[17] W. Fu, L. Sun, H. Cao, L. Chen, M. Zhou, S. Shen, Y. Zhu, S. Zhuang, Qualitative and Quantitative Recognition of Volatile Organic Compounds in Their Liquid Phase Based on Terahertz Microfluidic EIT Meta-Sensors, IEEE Sensors Journal 23 (12) (2023) 12775–12784.
[18] J. Xie, X. Zhu, X. Zang, Q. Cheng, L. Chen, Y. Zhu, Metamaterial-enhanced terahertz vibrational spectroscopy for thin film detection, Opt. Mater. Express 8 (1) (2018) 128.
[19] B. Han, Z. Han, J. Qin, Y. Wang, Z. Zhao, A sensitive and selective terahertz sensor for the fingerprint detection of lactose, Talanta 192 (2019) 1–5.
[20] Z. Han, A.M. Soehartono, B. Gu, X. Wei, K.-T. Yong, Y. Shi, Tunable hybridization induced transparency for efficient terahertz sensing, Opt Express 27 (6) (2019) 9032.
[21] S. Bhattacharyya, S. Ghosh, K.V. Srivastava, Equivalent circuit model of an ultra-thin polarization-independent triple band metamaterial absorber, AIP Adv. 4 (9) (2014), 097127.
[22] P.U. Jepsen, B.M. Fischer, Dynamic range in terahertz time-domain transmission and reflection spectroscopy, Opt. Lett. 30 (1) (2005) 29.
[23] A.B. Djurišić, E.H. Li, Modeling the index of refraction of insulating solids with a modified lorentz oscillator model, Appl. Opt. 37 (22) (1998) 5291.
[24] P. Sun, Y. Zou, Complex dielectric properties of anhydrous polycrystalline glucose in the terahertz region, Opt. Quant. Electron. 48 (1) (2016) 27.
[25] P. Weis, J.L. Garcia-Pomar, R. Beigang, M. Rahm, Hybridization Induced Transparency in composites of metamaterials and atomic media, Opt Express 19 (23) (2011), 23573.
[26] T. Chretiennot, D. Dubuc, K. Grenier, A microwave and microfluidic planar resonator for efficient and accurate complex permittivity characterization of aqueous solutions, IEEE Trans. Microw. Theor. Tech. 61 (2) (2013) 972–978.
[27] H.P. Schwan, Electrical properties of tissues and cell suspensions: mechanisms and models, in: Proceedings of 16th Annual International Conference of the IEEE Engineering in Medicine and Biology Society, IEEE, 1994, pp. A70–A71.
[28] G.A. Komandin, A.A. Gavdush, Yu G. Goncharov, O.E. Porodinkov, V.S. Nozdrin, S. V. Chuchupal, I.E. Spektor, Electrodynamical characteristics of α-lactose monohydrate in the terahertz range, Opt. Spectrosc. 126 (5) (2019) 514–522.
[29] M. Tal, S. Keren-Zur, T. Ellenbogen, Nonlinear plasmonic metasurface terahertz emitters for compact terahertz spectroscopy systems, ACS Photonics 7 (12) (2020) 3286–3290.
[30] E.R. Brown, J.E. Bjarnason, A.M. Fedor, T.M. Korter, On the strong and narrow absorption signature in lactose at 0.53THz, Appl. Phys. Lett. 90 (6) (2007), 061908.
[31] Z. Zhuan-Ping, F. Wen-Hui, Y. Hui, L. Jia, X. Li-Min, Study on THz spectra and vibrational modes of benzoic acid and sodium benzoate, Spectrosc. Spectr. Anal. 33 (3) (2013) 582–585.
[32] M. Walther, P. Plochocka, B. Fischer, H. Helm, P. Uhd Jepsen, Collective vibrational modes in biological molecules investigated by terahertz time-domain spectroscopy, Biopolymers 67 (4–5) (2002) 310–313.
[33] G. Zhao, B. Yu, C. Zhang, Terahertz spectroscopic investigation of four kinds of vitamins, J. Appl. Phys. 106 (10) (2009), 104702.
[34] L. Sun, M. Zhou, X. Wu, M. Yang, P. He, Detection of two isomers of dichloroaniline by terahertz time-domain spectroscopy, J. Terahertz Sci. Electron. Inf. Technol. 20 (5) (2022) 438.
[35] Y. Peng, J. Huang, J. Luo, Z. Yang, L. Wang, X. Wu, X. Zang, C. Yu, M. Gu, Q. Hu, X. Zhang, Y. Zhu, S. Zhuang, Three-step one-way model in terahertz biomedical detection, PhotoniX 2 (1) (2021) 12.
[36] J. Xu, D. Liao, M. Gupta, Y. Zhu, S. Zhuang, R. Singh, L. Chen, Terahertz microfluidic sensing with dual-torus toroidal metasurfaces, Adv. Opt. Mater. 9 (15) (2021), 2100024.
[37] L. Chen, D. Liao, X. Guo, J. Zhao, Y. Zhu, S. Zhuang, Terahertz time-domain spectroscopy and micro-cavity components for probing samples: a review, Front. Inf. Technol. Electron. Eng. 20 (5) (2019) 591–607.
[38] L. Chen, N. Xu, L. Singh, T. Cui, R. Singh, Y. Zhu, W. Zhang, Defect-induced fano resonances in corrugated plasmonic metamaterials, Adv. Opt. Mater. 5 (8) (2017), 1600960.
[39] J. Lyu, S. Shen, L. Chen, Y. Zhu, S. Zhuang, Frequency selective fingerprint sensor: the Terahertz unity platform for broadband chiral enantiomers multiplexed signals and narrowband molecular AIT enhancement, PhotoniX 4 (1) (2023) 28.

[40] Y. Wang, J. Zhang, M. Wang, G. Song, B. Zhang, B. Wei, Z. Ma, Y. Zhang, J. Lou, Q. Chen, Ultrasensitive metasurface-based sensors for fingerprint spectra extraction of L-glutamate at ultra-low concentration, Opt Commun. 550 (2024), 130005.
[41] Q. Wang, Q. Wang, Z. Yang, X. Wu, Y. Peng, Quantitative analysis of industrial solid waste based on terahertz spectroscopy, Photonics 9 (3) (2022) 184.
[42] Q. Yang, L. Wu, C. Shi, X. Wu, X. Chen, W. Wu, H. Yang, Z. Wang, L. Zeng, Y. Peng, Qualitative and quantitative analysis of caffeine in medicines by terahertz spectroscopy using machine learning method, IEEE Access 9 (2021) 140008–140021.